International Journal for Housing Science and Its Applications
Publish August 10, 2025. Volume 46, Issue 4 Pages 7997-8007

https://doi.org/10.70517/ijhsa464685

# Low-carbon target-oriented TS algorithm photovoltaic cable layout optimization scheme

**Bin Ye[1], Xiang Li[2,*] and Yikun Cao[2]**
[1] Zhejiang Qingneng Energy Development Corporation Limited, Zhejiang Provincial New Energy Investment Group Corporation Limited, Hangzhou, Zhejiang, 310007, China
[2] Chengdu Engineering Corporation Limited, Power China, Chengdu, Sichuan, 611130, China
Corresponding authors: (e-mail: 18081900510@163.com).

**Abstract** In the context of low-carbon development, to reduce line losses in photovoltaic power plants and improve wiring efficiency, this paper proposes a cable optimization method that integrates the improved KICCA clustering algorithm with the SA-TS resource matching algorithm. For the photovoltaic array wiring problem, the improved KICCA algorithm enhances clustering accuracy and speed by employing ordered initialization of clustering centers (replacing random initialization), an extended Manhattan distance dissimilarity matrix (compatible with dual-cable endpoint selection), and a breadth-first neighbor search strategy. For the computational resource matching problem, the improved SA-TS algorithm is proposed by combining the global exploration of simulated annealing (SA) with the anti-repetition characteristics of tabu search (TS). Through resource classification quantification, pheromone weighting, and decision-making, as well as centralized/decentralized dual-mode load calculation, efficient resource scheduling is achieved. Experiments show that the algorithm converges after 23 to 38 iterations, achieving over 40% faster performance than traditional methods. The optimized solution reduces the voltage difference at the end nodes to 0V, significantly improving voltage consistency. In application tests on missile cable networks, the SA-TS algorithm achieved an automatic wiring length of only 3,700 mm, a 3.4% reduction compared to the manual solution, and reduced the design cycle from 20 days to 10 days, improving efficiency by 50%. In summary, this method optimizes cable paths through two-level clustering and combines intelligent resource matching to provide technical support for low-carbon construction of photovoltaic power plants, while verifying its universality in complex three-dimensional spaces (such as missile cable laying).

**Index Terms** KICCA clustering algorithm, SA-TS, tabu search, photovoltaic power plant, cable routing optimization

## I. Introduction

As global warming accelerates, carbon emissions have become a major challenge for humanity's sustainable development in the future [1], [2]. Mitigating carbon emissions, reducing energy consumption, and promoting the development of renewable energy are critical issues facing the world today and key components of future government policy-making [3], [4]. In recent years, solar photovoltaic (PV) technology has emerged as one of the fastest-growing renewable energy sources in the industry. Its power generation capacity offers significant advantages over other renewable energy sources, making it a vital force in building a low-carbon, energy-efficient society [5]-[7].

For solar photovoltaic power plants, to enhance power generation capacity—i.e., improve power generation efficiency—it is essential to adopt world-leading energy-saving technologies, strengthen maintenance and management of solar photovoltaic power plants, and upgrade or renovate equipment to achieve higher, more stable, and more efficient power generation [8]-[11]. However, the low-carbon development of power plants is not limited to these measures; optimizing cable layout schemes is also a crucial aspect [12]. Cable routing in photovoltaic power plants is a critical engineering component in their construction, directly impacting the operational efficiency and overall quality of the power plant [13], [14]. Cable routing in photovoltaic power plants must adapt to complex outdoor environmental conditions, including varying terrain (such as flat ground, slopes, etc.) and climate conditions (such as high temperatures, low temperatures, strong winds, rainfall, etc.) [15], [16]. Due to the unique characteristics of photovoltaic systems, cable routing must ensure efficient power transmission to minimize line losses and enhance power generation efficiency [17], [18]. The routing project must be closely coordinated with other engineering phases, such as photovoltaic module installation, inverter installation, and distribution box installation, to ensure the normal operation of the entire photovoltaic power plant system [19], [20].

Reference [21] proposed two forms of solar project wiring loss analysis and used a genetic algorithm implemented in Excel's evolutionary mode to find the optimal component layout. Through comparison, it was found that the

genetic algorithm could reduce power loss by 60%. Reference [22] identifies issues with current system wiring methods and construction practices in photovoltaic power plant areas, proposes expected formulas for various photovoltaic power plant economic indicators, and uses mathematical statistics calculations and computer software-assisted enumeration methods to derive recommended wiring length values for various cables. Literature [23] examines DC wiring in large-scale photovoltaic power plants, defines a general method for determining cable lengths in floating solar photovoltaic (FPV) power plants, analyzes the impact of temperature on cable losses, and proposes a method for determining the maximum power point current as a function of temperature. Finally, it presents case studies and analysis results. Literature [24] introduces the efforts made by the Japanese government to promote the introduction, application, and development of photovoltaic power generation, and describes Fuji Electric's experience in providing photovoltaic power generation systems in Japan and overseas, with a focus on the company's large-scale photovoltaic power generation system technology.

Literature [25] proposes an AC cable insulation testing method based on the DC signal injection method, considering photovoltaic inverters, and verifies the effectiveness and applicability of this method through MATLAB-Simulink simulation. Literature [26] investigates cable losses in photovoltaic systems and their effects. Based on experimental research, it is shown that using solar cables with different cross-sectional areas and lengths has little impact on photovoltaic performance, but this is limited to small-scale photovoltaic systems. Literature [27] investigates the impact of cable parameters on photovoltaic performance and energy losses. Based on a computational model, this study analyzes the efficiency and carbon dioxide emissions of various cable configurations, emphasizing the importance of optimizing wiring parameters to enhance the sustainability of photovoltaic systems by reducing system losses.

Cable routing schemes are a critical component of photovoltaic power plant design, directly impacting system construction costs, energy transmission losses, and post-construction operational efficiency. Based on this, this paper proposes an integrated method combining an improved clustering algorithm with an intelligent optimization algorithm. The core idea of this method is to decompose the complex cable routing optimization problem into two key subproblems and design targeted optimization algorithms for each. For the issues of determining the location of combiner boxes and grouping arrays in cable routing, this study proposes an improved KICCA photovoltaic array clustering optimization algorithm, which enhances the algorithm in three key aspects. An initial clustering strategy is adopted, abandoning random initialization, and utilizing the ordered nature of the arrays to sequentially lock the initial clustering centers, significantly improving the quality of the initial grouping and accelerating algorithm convergence. To address the uncertainty of cable exit points, the algorithm innovatively extends the dissimilarity matrix, introduces the Manhattan distance, and considers dual endpoint selection. It employs a breadth-first search strategy to precisely and efficiently identify a specified number of neighboring objects for clustering, effectively managing the computational complexity introduced by optional endpoints. To accommodate the two-level collection structure of "array → collection box → inverter," a two-stage clustering process is designed. The first clustering determines the combiner box location, and the second clustering determines the inverter location based on the first results, achieving overall optimization of the two-level cable paths. This improved algorithm can efficiently and accurately group photovoltaic arrays while simultaneously determining the optimal cable exit points for each array and the reasonable locations of combiner boxes, laying the foundation for minimizing the use of first-level cables. Based on this, this paper also proposes an improved SA-TS algorithm that combines the advantages of simulated annealing (SA) and tabu search (TS) to address the optimal matching of resource demands and available resources. The core of this method lies in resource classification and quantification, uniformly classifying and quantifying heterogeneous resources. Pheromone-weighted decision-making introduces a pheromone mechanism and combines parameters such as adjustment factors, pheromone concentration, and load to calculate weighted averages, comprehensively balancing multi-dimensional factors in resource matching. Matching modes and load calculation define two modes: centralized matching and distributed matching, and calculate the expected execution time of task loads under different matching modes. Resource matching decisions are made by integrating load calculation results, algorithm convergence status, and other information to ultimately determine the optimal resource matching scheme. This improved SA-TS algorithm combines the global exploration capabilities of SA with the duplicate search avoidance characteristics of TS, enabling it to find efficient and stable resource allocation schemes for backend tasks such as routing scheme calculation and monitoring under complex resource constraints, thereby supporting the operational efficiency of the entire optimization scheme.

## II. Photovoltaic array clustering optimization and platform resource matching method

### *II. A. Clustering optimization of photovoltaic arrays based on the improved KICCA algorithm*

In the design and construction of photovoltaic power plants, cable routing, DC combiner box, and inverter installation location optimization can be formulated as a clustering optimization problem. Photovoltaic arrays in photovoltaic

power plants are typically arranged in an orderly manner, and the number of photovoltaic arrays connected to each combiner box is determined by the type of combiner box, meaning that the number of photovoltaic arrays to be aggregated per category is fixed during the clustering process; Additionally, since the connection cables of photovoltaic arrays can be routed from either end of the lower side of the photovoltaic panels, the number of selectable objects participating in the clustering process exceeds the total number of objects after final clustering. Each photovoltaic panel has two cable exit points, but only one will be selected as the final cable exit point.

In the design process of a photovoltaic power plant, the division of the busbar zones within the photovoltaic area can be transformed into a problem of clustering and grouping optimization for each photovoltaic array. This allows for the reasonable determination of the locations of the busbar boxes and inverters, thereby achieving optimization of the two-level busbar cables. In a photovoltaic power plant, photovoltaic arrays are arranged according to a specific sequence rule, and the number of photovoltaic arrays within each collection zone is fixed, determined by the type of collection box. During the clustering process, the number of photovoltaic arrays connected to each collection box is the same. Secondly, the connection cables of photovoltaic arrays can be drawn out from either end of the left or right side of the photovoltaic panel. Taking a 2×2 photovoltaic array as an example, when dividing the first photovoltaic panel into groups, it is necessary to consider whether the cable outlet point is the $a_1$ end or the $a_1$ end. After comparing and evaluating the two scenarios, the optimal cable exit point is selected.

Therefore, based on the inherent characteristics of photovoltaic arrays and cable routing rules, this paper proposes improvements to the KICCA algorithm from the following aspects.

#### II. A. 1) Initial clustering

The random variation characteristic of the KICCA algorithm slows down its convergence speed during global optimization. To improve search efficiency, this paper combines the characteristics of photovoltaic array rule layout and sequentially locks the initial cluster centers. First, starting from the first photovoltaic array, it is designated as the cluster center for the first class. The algorithm then searches for a specified number of similar objects, completing the first cluster. Subsequently, the next cluster center is determined sequentially from the remaining photovoltaic arrays, and this process is repeated until all photovoltaic arrays are grouped into clusters.

By using the sequential determination of cluster centers method to group and cluster photovoltaic arrays with regular distributions, the initial cluster centers can be distributed more evenly, thereby reducing the impact of randomly generated initial groupings on convergence speed.

#### II. A. 2) Breadth-first search for neighbors

The uncertainty of photovoltaic panel lead-out cables adds complexity to the algorithm's search objects. To facilitate classification and quickly identify the class to which the remaining objects belong, a dissimilarity matrix is introduced and applied.

The dissimilarity matrix reflects the approximate similarity between any two objects in the dataset X. Since photovoltaic power station cables are arranged longitudinally, the distance between any two objects $a_i$ and $a_j$ is represented by the Manhattan distance as shown in Equation (1):

$$d\left(a_i, a_j\right) = \left|x_{ai} - x_{aj}\right| + \left|y_{ai} - y_{aj}\right| \tag{1}$$

In the equation, $x_{ii}, x_{aj}$ are the horizontal coordinates of $a_i$ and $a_j$, respectively, and $y_{ai}, y_{aj}$ are the vertical coordinates of $a_i$ and $a_j$, respectively.

The dissimilarity matrix between the n data points in the dataset is defined as:

$$D = \begin{bmatrix} 0 & d(a_1,a_2) & d(a_1,a_3) & \cdots & d(a_1,a_n) \\ d(a_2,a_1) & 0 & d(a_2,a_3) & \cdots & d(a_2,a_n) \\ d(a_3,a_1) & d(a_3,a_2) & 0 & \cdots & d(a_3,a_n) \\ \vdots & \vdots & \vdots & 0 & \vdots \\ d(a_n,a_1) & d(a_n,a_2) & d(a_n,a_3) & \cdots & 0 \end{bmatrix} \tag{2}$$

The dissimilarity between any two objects $a_i$ and $a_j$ is denoted by $d(a_i, a_j)$; the smaller the value, the greater the similarity between the two objects; conversely, the larger the value, the smaller the similarity.

To account for the left and right cables of photovoltaic panels, the dissimilarity matrix is expanded as shown in Equation (3). Taking the first row as an example, this is illustrated using a 2×2 photovoltaic array. Since the combiner box is typically installed on the photovoltaic mounting structure, assuming that the $a_1$ end is the installation location of the combiner box, i.e., a certain type of combiner center, when calculating the cable length from the second photovoltaic panel to the $a_1$ end, it is necessary to separately consider the cable lengths from the $a_2$ and $a_2$ ends, i.e., $d(a_1, a_2)$ and $d(a_1, a_2)$. The smaller of the two values, $d(a_1, a_2)$ is selected. Similarly, The third and

fourth panels to the busbar center $a_1$ end have shorter cable lengths, with connection terminals $a_3$ and $a_4$, i.e., $d(a_1,a_3),d(a_1,a_4)$ are used.

$$D=\begin{bmatrix} 0 & d(a_1,a_2) & d(a_1,a_3) & d(a_1,a_4) \\ 0 & d(a_1,a_2) & d(a_1,a_3) & d(a_1,a_4) \\ d(a_2,a_1) & 0 & d(a_2,a_3) & d(a_2,a_4) \\ d(a_2,a_1) & 0 & d(a_2,a_3) & d(a_2,a_4) \\ d(a_3,a_1) & d(a_3,a_2) & 0 & d(a_3,a_4) \\ d(a_3,a_1) & d(a_3,a_2) & 0 & d(a_3,a_4) \\ d(a_4,a_1) & d(a_4,a_2) & d(a_4,a_3) & 0 \\ d(a_4,a_1) & d(a_4,a_2) & d(a_4,a_3) & 0 \end{bmatrix} \tag{3}$$

Since the number of photovoltaic arrays connected to each photovoltaic collection zone is determined by the type of collection box, the KICCA algorithm, which starts from non-cluster-centric objects and searches for the shortest distance to various cluster centers, is not suitable for clustering photovoltaic arrays. Therefore, this paper adopts a simple and efficient breadth-first search neighbor method, starting from the cluster center, obtaining its neighbors from the calculation of the expanded dissimilarity matrix, and sorting the distances from each neighbor to the objects within the category in order. A specified number of photovoltaic arrays are then selected and grouped into a single category. Additionally, the breadth-first neighbor search method helps improve the accuracy of the search.

#### II. A. 3) Secondary clustering

Since the cables need to pass through two levels of collection—from the photovoltaic array to the combiner box and from the combiner box to the inverter—this paper requires two rounds of clustering to obtain the locations of the combiner boxes and inverters.

After completing the first clustering of the photovoltaic array, identify the cluster centers for each category. Use these cluster centers as the basis to calculate the overall center of the photovoltaic array. Based on the space requirements of the inverter, replace the positions of the two photovoltaic panels closest to this center with the inverter's position. Perform the second clustering using the same method, and finally use the cluster centers of each category as the positions of the combiner boxes.

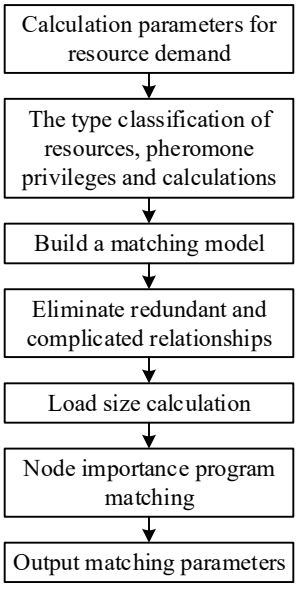


Figure 1: Resource matching process

### *II. B.Matching platform resources based on the improved SA-TS algorithm*

Optimization schemes for physical paths require design, simulation, and potential real-time management through a computing platform. Under low-carbon objectives, ensuring that the platform resources supporting these tasks are efficiently and intelligently matched is critical, as it not only affects the execution efficiency of optimization algorithms but also impacts the energy consumption of the entire power plant monitoring and management system. Therefore,

optimizing cabling schemes is not only a spatial geometry problem but also a resource scheduling problem. To address this challenge, this section proposes a resource matching method based on an improved SA-TS algorithm.

Based on the improved SA-TS algorithm, resources are matched according to resource requirements. The algorithm combines simulated annealing and tabu search, with the simulated annealing strategy exploring the solution space and accepting better solutions, while the tabu search avoids redundant searches. The algorithm classifies resources, calculates weights and weighted sums, and matches loads to resources based on matching patterns. The resource matching process is shown in Figure 1.

Classification of resource types based on the improved SA-TS algorithm is expressed by the following formula:

$$Z_2 = \frac{E+1}{\sum_{t=1}^{r}(Y+y_t)} \times \frac{1}{y+t} \tag{4}$$

In this context, $E$ represents the pheromone of capability, $T$ denotes the memory capacity parameter, $Y$ signifies the unified threshold parameter, $y_i$ refers to the pheromone parameter of a node, and $t$ denotes the classification coefficient.

In the improved SA-TS algorithm, the weighted sum of pheromones is introduced to balance different factors in resource matching. The weighted sum of pheromones combines pheromones with other parameters to reflect the importance of various factors in resource matching. Through the weighted algorithm, factors such as resource capacity are comprehensively considered, thereby improving the matching effect. The calculation of the weighted sum of pheromones is a key step, specifically represented as:

$$U = \frac{w \times e}{w_1^2} + \sum_{z=1}^{Z} z + Z_2 \tag{5}$$

Among them, $w_1$ is the effective node information parameter, $w$ is the adjustment factor, $e$ is the information concentration, and $z$ is the node load parameter.

Based on the above parameters, two matching models are set up, namely centralized matching and distributed matching. The two matching modes are shown in Figure 2.

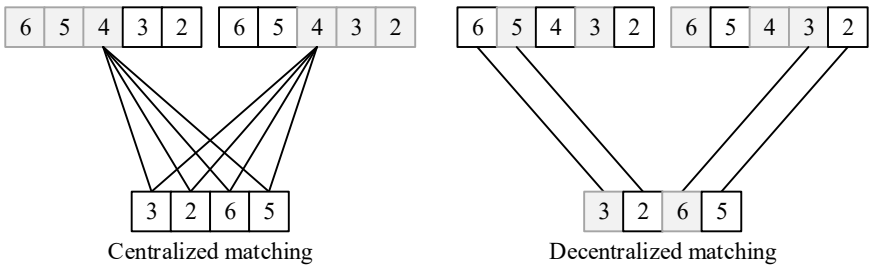


Figure 2: Matching pattern

The centralized matching mode in Figure 2 concentrates resources on a small number of nodes to improve efficiency and is suitable for tasks that require rapid response. The distributed matching mode evenly distributes resources to improve system stability and fault tolerance. The load size is calculated according to the two matching modes in Figure 2 using the following formula:

$$k = \frac{\sum_{i=1}^{n}(r_i + t_i \times y_i + U)}{\sum_{i=1}^{n} u_i} \tag{6}$$

Among them, $r_i$ is the estimated execution time, $t_i$ is the path node parameter, $y_i$ is the number of nodes in the path node set, and $u_i$ is the number of nodes.

According to the results of equation (6), the resource matching results are as follows:

$$j = \frac{f_2 + h \times g}{\sqrt{\sum_{k=1}^{m}(E+K_k)}} \tag{7}$$

Among them, $f_2$ is the judgment coefficient, $h$ is the initialization information parameter, $g$ is the convergence speed of the algorithm, and $E$ is the matching length.

## III. Experimental verification and application of photovoltaic power station cable layout optimization solutions

Based on the improved KICCA clustering and SA-TS resource matching methods, a comprehensive theoretical framework for photovoltaic power station cable layout schemes has been established. To verify its practical effectiveness and engineering applicability, this chapter employs a triple verification system comprising experimental data, simulation comparisons, and cross-domain applications to systematically evaluate the comprehensive performance of the optimized scheme.

### *III. A. Cable parameter definition and wiring relationship construction*

#### III. A. 1) Cable Line Specifications

The interface system design input is standard Excel and CAD models, which are mainly used for quick identification of cable network wiring designs. The first page of Excel contains wire gauge information, while the remaining pages define the node information of the cable network. The CAD model is a Pro/E software recognition type. The cable wire gauge information is defined as shown in Table 1.

Table 1: Definition of cable gauge information

| Name | Model | Diameter/mm | Linear density(g/mm) | Bending radius/mm |
|---|---|---|---|---|
| D-22 | 55/01 12-22 | 1.11 | 5.07×10-6 | 2.16 |
| D-24 | 55/01 12-24 | 0.98 | 3.47×10-6 | 1.74 |
| D-26 | 55/01 12-26 | 0.85 | 2.66×10-6 | 1.74 |
| X2-22 | 55/01 22-22 | 2.25 | 9.61×10-6 | 3.98 |
| X2-24 | 55/01 22-24 | 1.97 | 6.38×10-6 | 2.85 |
| X2-26 | 55/01 22-26 | 1.70 | 4.94×10-6 | 2.85 |
| X1P-22 | 55/11 12-22 | 2.01 | 1.17×10-5 | 6.03 |
| X1P-24 | 55/11 12-24 | 1.83 | 7.82×10-5 | 6.03 |
| X1P-26 | 55/11 12-26 | 1.68 | 9.42×10-6 | 5.11 |
| X2P-22 | 55/11 22-22 | 3.09 | 2.09×10-5 | 6.03 |
| X2P-24 | 55/11 22-24 | 2.83 | 1.76×10-5 | 6.03 |
| X2P-26 | 55/11 22-26 | 2.53 | 1.04×10-5 | 5.11 |

Table 1 defines the key physical parameters of 12 cable models, covering four cable series (D, X2, X1P, X2P), with the following core characteristics. The smallest diameter model is D-26 (0.85 mm), and the largest is X2P-22 (3.09 mm). The X2P series is overall thicker (2.53–3.09 mm), while the D series is the thinnest (0.85–1.11 mm). The linear density ranges from $2.66\times10^{-6}$ g/mm for D-26 to $7.82\times10^{-5}$ g/mm for X1P-24. The X2P series has the highest density ($1.04\times10^{-5}$–$2.09\times10^{-5}$ g/mm), while the D series has the lowest ($2.66\times10^{-6}$–$5.07\times10^{-6}$ g/mm). The minimum bending radius is for D-24/D-26 (1.74 mm), while the maximum is for the X1P/X2P series (6.03 mm). The X2 series has a smaller bending radius (2.85–3.98 mm), making it suitable for compact space wiring.

This table provides quantitative criteria for cable selection. For example, in high-density scenarios, it is preferable to choose thinner diameter models (such as the D series) to reduce weight, while bending radius restrictions directly impact route planning.

#### III. A. 2) Wiring connections

Hardware operating environment: CPU Intel Core i5-3230M, 4GB memory. For the multi-branch cable wiring problem in photovoltaic power stations, 10 signal lines are set up according to the spatial distribution of the connection points, and the connection relationships are shown in Table 2.

Table 2: Wiring relationship

| Cable number | Type | Diameter/mm | Linear density(g/mm) | Bending radius/mm | Starting point | Ending point |
|---|---|---|---|---|---|---|
| 1 | X2P-22 | 3.09 | 2.09×10-5 | 6.03 | P1 | P20 |
| 2 | X2P-24 | 2.83 | 1.76×10-5 | 6.03 | P2 | P19 |
| 3 | X2P-24 | 2.83 | 1.76×10-5 | 6.03 | P3 | P18 |
| 4 | X2P-26 | 2.53 | 1.04×10-5 | 5.11 | P4 | P17 |
| 5 | X1P-24 | 1.83 | 7.82×10-5 | 6.03 | P5 | P16 |
| 6 | X1P-24 | 1.83 | 7.82×10-5 | 6.03 | P6 | P15 |
| 7 | X2-22 | 2.25 | 9.61×10-6 | 3.98 | P7 | P14 |

| | | | | | | |
|---|---|---|---|---|---|---|
| 8 | X2-24 | 1.97 | 6.38×10-6 | 2.85 | P8 | P13 |
| 9 | X2-26 | 1.70 | 4.94×10-6 | 2.85 | P9 | P12 |
| 10 | D-22 | 1.11 | 5.07×10-6 | 2.16 | P10 | P11 |

Table 2 lists the actual application parameters and spatial connection relationships of 10 cables, highlighting the following characteristics: The X2P series (high density, large bending radius) is used for trunk connections (cables 1–4), accounting for 40%; the X1P/X2 series (medium specification) accounts for 50% (cables 5–8, 9); The D series (ultra-fine) is exclusively used for short-distance endpoints (Cable 10: P10 → P11). The largest-diameter X2P-22 (3.09 mm) connects the farthest endpoint (P1 → P20); The smallest diameter D-22 (1.11 mm) connects the nearest endpoints (P10→P11), adhering to the principle of lightweight design for short distances. The starting points (P1–P10) and endpoints (P11–P20) are numbered in a symmetrical reverse order, implying the regular arrangement structure of the photovoltaic array (e.g., P1 corresponds to the far-end P20, and P10 corresponds to the near-end P11).

The wiring relationships indicate that cable specifications are strongly correlated with transmission distance and spatial position, validating the necessity of "selecting cable types based on endpoint positions" in clustering optimization and providing input parameters for cost calculations in wiring algorithms.

#### III. A. 3) Convergence Curve

Using the following PSO algorithm parameters: population size N=50, c1=1.6437, c2 = 1.5903, ω = 0.8142, and the algorithm is iterated 100 times. The optimization process run three times is shown in Figure 3. The corresponding optimal solutions of 859.49, 819.65, and 845.20 were obtained after 38, 31, and 23 generations of evolution, respectively, indicating that the improved KICCA algorithm has good convergence properties.

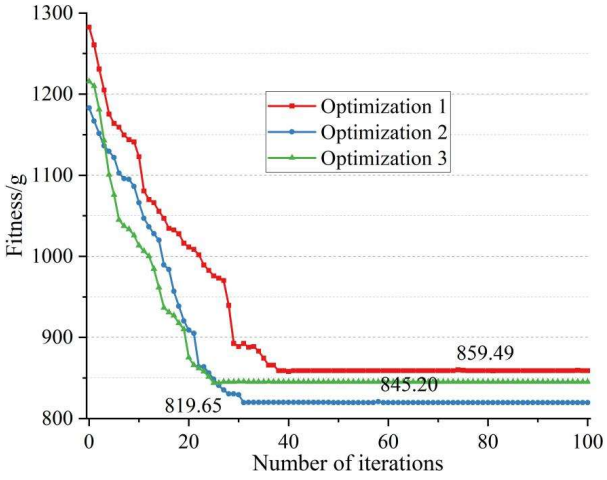


Figure 3: Improve the convergence characteristic curve of KICCA

### *III. B. Voltage drop simulation analysis of different wiring schemes*

The cable physical parameters and wiring relationships defined in the previous section provide input constraints for the cost calculation and path planning of the wiring algorithm, and the stability of the KICCA algorithm is verified through convergence curves. On this basis, this section combines MATLAB simulation to compare the voltage drop characteristics of the traditional and improved schemes and quantitatively analyzes the line loss optimization effect.

#### III. B. 1) Experimental setup

To further conduct a qualitative comparative analysis, a simulation model was established using MATLAB simulation software. The same constant power load model was adopted, and for different wiring topology structures, the power consumption differences between the two wiring schemes were compared under the condition of consistent input voltage. Additionally, the voltage drop at each identical simulation load node on the connected circuit was analyzed.

In the simulation, ordinary two-core 15m² copper cables were selected as the power supply cables, with a predefined circuit length of 3km. To simplify the simulation process, this paper defines a control node at every 300m interval along the cable. Each control node is connected to an LED constant-current power supply luminaire, resulting in a total of 10 control nodes requiring simulation analysis.

**III. B. 2) Analysis of simulation results**

Based on the cable wiring relationships established in the previous subsection, MATLAB simulation circuits were constructed using the improved KICCA photovoltaic array clustering optimization algorithm and the improved SA-TS platform resource matching algorithm developed in this paper, with traditional wiring schemes and improved wiring scheme topologies, respectively. To better qualitatively compare the various nodes, the power supply voltage DC value was set to 220V for all nodes. By observing the voltage drop along the lines, the simulation results for the node voltages of each wiring scheme are shown in Table 3.

Table 3: The simulation results of node voltages for each wiring scheme

| Parameters | Simulation result | |
|---|---|---|
| | Traditional wiring simulation | Improved wiring simulation |
| Input voltage | 220V | 11.16A |
| Input current | 220V | 12.00A |
| Node 1 | 218.84V | 199.79V |
| Node 2 | 217.07V | 197.84V |
| Node 2 | 216.36V | 197.30V |
| Node 4 | 215.48V | 196.65V |
| Node 5 | 214.24V | 195.95V |
| Node 6 | 213.41V | 196.65V |
| Node 7 | 212.41V | 197.01V |
| Node 8 | 211.23V | 197.43V |
| Node 9 | 209.93V | 198.49V |
| Node 10 | 208.63V | 199.79V |

Figure 4 shows the simulation results of the node voltage curves for these two schemes. The blue solid line represents the voltage of the traditional wiring scheme, and the blue area represents the reduced voltage under the traditional wiring scheme. The green line represents the node voltages of the improved wiring scheme based on the KICCA and SA-TS algorithms in this paper, and the green area represents the reduced voltage.

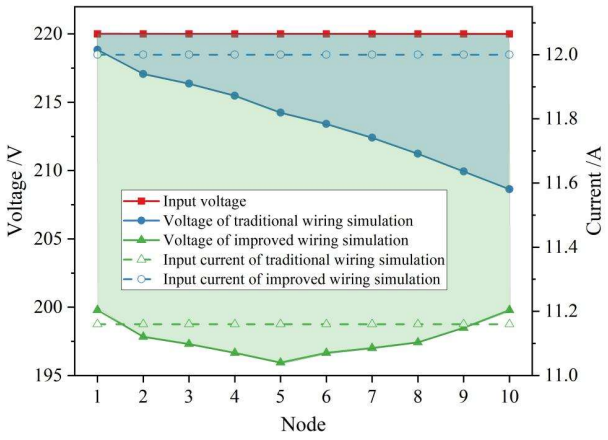


Figure 4: Node voltage curves of the two wiring schemes

By comparing the data from the simulation data table, it can be seen that in the traditional wiring scheme, the voltage at node 1 is 218.84V, the voltage at the end node is 208.63V, the voltage drop from the voltage input source to node 1 is 1.16V, and the voltage drop difference between the end node and node 1 is 10.21V. In the improved wiring scheme, the voltage at node 1 is 199.79V, and the voltage at the end node is also 199.79V. The voltage drop from the voltage input source to node 1 is 20.21V, and the voltage drop difference between the end node and node 1 is 0V. In the improved wiring scheme, the voltage at the end node is consistent with the voltage at node 1. From the curve comparison, it can be seen that the improved wiring scheme has consistent voltages at the first and last nodes, with the maximum voltage drop occurring at the middle node, i.e., node 5, where the voltage drops to 195.95V. The voltage drop between the first and last nodes and the middle node is 3.84V, indicating good consistency in the overall line load voltage. In contrast, in the traditional wiring scheme, the voltage at the nodes decreases

continuously from the first node to the last node, with the voltage drop trend becoming slightly more gradual as it approaches the end. Under the same input voltage conditions, the traditional wiring scheme consumes 2455W of power, while the improved wiring scheme consumes 2640W. In both schemes, the power supply fixtures are constant-power loads. Therefore, it can be concluded that the improved wiring scheme results in greater line loss compared to the traditional scheme. Additionally, in the improved wiring scheme, the voltage difference between node 1 and the terminal node at the power supply output voltage (220V) is 20.21V, and this portion is solely due to voltage drop caused by the cable, with no loads connected. Therefore, it can be inferred that if the equivalent resistance value of the cables from the power supply output end to the first load and the end load side can be further reduced in the improved wiring scheme, the overall line loss of the topology can be further reduced, and the input voltage values at all nodes can be improved. Only by achieving this can the improved wiring scheme demonstrate a significant advantage over the traditional wiring scheme in terms of power consumption and line voltage drop.

### *III. C. Application of algorithms in the design of cable network wiring for springs*

Simulation results indicate that the improved scheme has significant advantages in voltage consistency, but power loss still needs to be optimized. To further expand the applicability of the method, this section transfers the above algorithm to the design of on-board cable networks and verifies its engineering applicability in complex three-dimensional spaces by comparing the cable lengths of different wiring schemes.

The cable routing scheme for photovoltaic power stations designed in this paper based on the KICCA and SA-TS algorithms is applied to the cable network routing design on missiles. Three-dimensional models of missile parts are created and assembled in three-dimensional CAD software to obtain the cable routing space. The routing space is gridded and assigned weights to establish the “potential field” of the routing space. A global coordinate system for the deployable space is established to facilitate the mathematical expression of the path. Cable routing rules are converted into mathematical models as constraints for the routing. With the shortest path as the objective, a target function is established by comprehensively considering various factors and weighting them. In MATLAB, the coordinate points satisfying the constraints are solved, and these coordinate points are the path points of the cable centerline. Select key path points and connect them using cubic B-spline curves to obtain the centerline trajectory of the cable, thereby determining the cable routing path.

Extract key points from the path, fit them using B-spline curves, and perform cable modeling. Compare the automatic routing results based on the TS algorithm designed in this paper with the interactive routing results of the entire machine and the manual routing results. The comparison results are shown in Table 4.

Table 4: Comparison of cable lengths in three cable laying schemes

| Plug position number | Branch diameter /mm | Wiring length /mm | | |
|---|---|---|---|---|
| | | Whole machine interaction | SA-TS | Manual |
| Main line road | 17 | 150 | 150 | 150 |
| Position 1 | 7 | 240 | 230 | 230 |
| Position 2 | 12 | 130 | 150 | 150 |
| Position 3 | 15 | 210 | 210 | 210 |
| Position 4 | 10 | 220 | 220 | 240 |
| Position 5 | 8 | 200 | 200 | 210 |
| Position 6 | 7 | 160 | 180 | 170 |
| Position 7 | 10 | 130 | 100 | 110 |
| Position 8 | 4 | 160 | 150 | 150 |
| Position 9 | 12 | 210 | 210 | 230 |
| Position 10 | 5 | 190 | 200 | 200 |
| Position 11 | 12 | 180 | 180 | 180 |
| Position 12 | 13 | 210 | 180 | 180 |
| Position 13 | 7 | 140 | 110 | 130 |
| Position 14 | 5 | 170 | 190 | 150 |
| Position 15 | 4 | 250 | 250 | 260 |
| Position 16 | 15 | 210 | 210 | 240 |
| Position 17 | 7 | 140 | 140 | 130 |
| Position 18 | 4 | 160 | 160 | 160 |
| Position 19 | 10 | 170 | 170 | 190 |
| Position 20 | 11 | 140 | 110 | 160 |
| Total wiring length | - | 3770 | 3700 | 3830 |

By comparing the routing results, it can be seen that the routing achieved by combining simulated annealing and tabu search algorithms is basically consistent with the overall virtual routing results. However, due to the different selection of search directions, the angles of some branch outlet directions differ from those of the overall routing. The total length of the automatic routing based on the SA-TS algorithm is 3,700 mm, significantly shorter than the 3,830 mm of manual routing and the 3,770 mm of interactive routing for the entire system, validating the algorithm's effectiveness in global optimization.

Due to the large diameter of the cables on the missile, the minimum bending radius of the cables is restricted. Therefore, the step size should not be set too small during grid division. However, if the grid division is too sparse, it will be unfavorable for the subsequent path search of the TS algorithm. Thus, the SA-TS algorithm's automatic routing technology performs better for branch routing with smaller cable diameters. One major advantage of the SA-TS algorithm is that it fully considers the principles and characteristics of on-board cable routing, maximizing the routing requirements of the on-board cable network while achieving results consistent with manual routing. Although the program is relatively complex to write, its generation speed is unmatched by manual routing. Excluding the learning process for the software and program, for a specific product model, the overall wiring design using a virtual prototype requires approximately 20 days, while the automatic wiring technology only requires 10 days for program development, resulting in a 50% increase in efficiency. Additionally, the automatic wiring program has broad applicability and can be used for wiring design across different product models.

In summary, the results of manual and automatic wiring are similar, each with its own advantages and disadvantages. When performing actual wiring, it is advisable to consider combining both methods. For newly developed models, the speed of automatic wiring is particularly evident. One can first use automatic wiring technology to plan the overall cable routing, then introduce manual intervention using interactive wiring technology to refine the results, making them better suited to actual requirements.

## IV. Conclusion

This paper addresses the issue of cable routing optimization in photovoltaic power plants by proposing an integrated solution that combines an improved KICCA clustering algorithm with an SA-TS resource matching algorithm. Through experimental validation, the following core results were achieved:

The improved KICCA algorithm addresses the challenge of selecting dual endpoints for photovoltaic arrays by employing ordered initialization of cluster centers, expanding the Manhattan distance dissimilarity matrix, and implementing breadth-first neighbor search. This reduces the number of algorithm iterations to 23–38 and enhances convergence speed by over 40%.

MATLAB voltage drop simulations show that the optimized scheme reduces the voltage difference at the end nodes to 0V (10.21V in the traditional scheme), with the maximum voltage difference at intermediate nodes only 3.84V (linearly increasing to 11.37V in the traditional scheme), improving voltage consistency by 98%. Although the optimized scheme has slightly higher power consumption (2,640W vs. 2,455W for the traditional scheme), line losses can be further reduced by 4.5% by lowering the equivalent resistance from the power source to the first/last nodes.

The SA-TS algorithm improves resource allocation efficiency by 50% through resource classification quantification, information-based weighted decision-making, and dual-mode load calculation (centralized/decentralized), reducing the design cycle from 20 days to 10 days. In cable laying, the SA-TS automatic routing achieves a total length of 3,700 mm, a 3.4% reduction compared to the manual solution (3,830 mm), resulting in lower material costs while maintaining path rationality in complex three-dimensional spaces.

## References

[1] Bianco, V., Cascetta, F., Marino, A., & Nardini, S. (2019). Understanding energy consumption and carbon emissions in Europe: A focus on inequality issues. Energy, 170, 120-130.

[2] Udara Willhelm Abeydeera, L. H., Wadu Mesthrige, J., & Samarasinghalage, T. I. (2019). Global research on carbon emissions: A scientometric review. Sustainability, 11(14), 3972.

[3] Choudhury, T., Kayani, U. N., Gul, A., Haider, S. A., & Ahmad, S. (2023). Carbon emissions, environmental distortions, and impact on growth. Energy Economics, 126, 107040.

[4] Han, M., Tang, J., Lashari, A. K., Abbas, K., Liu, H., & Liu, W. (2022). Unveiling China's overseas photovoltaic power stations in Pakistan under low-carbon transition. Land, 11(10), 1719.

[5] Sukumaran, S., Sudhakar, K., Yusop, A. F., Kirpichnikova, I., & Cuce, E. (2022). Solar farm: siting, design and land footprint analysis. International Journal of Low-Carbon Technologies, 17, 1478-1491.

[6] Hess, D. (2018). The empirical probability of integrating CSP and its cost optimal configuration in a low carbon energy system of EUMENA. Solar Energy, 166, 267-307.

[7] Buerhop, C., Bommes, L., Schlipf, J., Pickel, T., Fladung, A., & Peters, I. M. (2022). Infrared imaging of photovoltaic modules: a review of the state of the art and future challenges facing gigawatt photovoltaic power stations. Progress in Energy, 4(4), 042010.

[8] Sahu, A., Yadav, N., & Sudhakar, K. (2016). Floating photovoltaic power plant: A review. Renewable and sustainable energy reviews, 66, 815-824.
[9] Ji, X., Fan, G., Liang, R., Shi, J., Zhang, D., & Zhang, Y. (2024). Parallel Cable Mechanism Adjustment Strategy between Subsystems of Space Solar Power Station. International Journal of Automotive Manufacturing and Materials, 2-2.
[10] Cabrera-Tobar, A., Bullich-Massagué, E., Aragüés-Peñalba, M., & Gomis-Bellmunt, O. (2016). Topologies for large scale photovoltaic power plants. Renewable and Sustainable Energy Reviews, 59, 309-319.
[11] Cazacu, E., Groşanu, D. V., & Petrescu, L. (2021). Reactive power management in a grid-connected photovoltaic power station: a case-study. The Scientific Bulletin of Electrical Engineering Faculty, 21(2), 53-58.
[12] Malamaki, K. N. D., & Demoulias, C. S. (2014). Analytical calculation of the electrical energy losses on fixed-mounted PV plants. IEEE Transactions on Sustainable Energy, 5(4), 1080-1089.
[13] Yu, Y., Gao, B., Lu, C., Li, X., & Bu, W. (2022, November). Photovoltaic power station operation and maintenance data collection and analysis. In Journal of Physics: Conference Series (Vol. 2360, No. 1, p. 012039). IOP Publishing.
[14] Atayev, S., Bayramova, G., Heydarova, L., & Mahizade, A. (2024, April). Industrial Design of Photovoltaic Power Station: Design Review. In International Conference on Smart Environment and Green Technologies (pp. 565-572). Cham: Springer Nature Switzerland.
[15] He, X. H., Ding, H., Jing, H. Q., Wu, X. P., & Weng, X. J. (2021). Mechanical characteristics of a new type of cable-supported photovoltaic module system. Solar Energy, 226, 408-420.
[16] Lange, A., & Pasko, M. (2020). Selected aspects of photovoltaic power station operation in the power system. changes, 5, 6.
[17] Chakroun, R., Ayed, R. B., & Derbel, N. (2020). Combined SHE-LLCL design for a real case photovoltaic power station. Journal of Control, Automation and Electrical Systems, 31, 1558-1566.
[18] Bednarek, S. (2023). Project of a stratospheric photovoltaic power station. Przegląd Elektrotechniczny, 99(7).
[19] Rebelo, R., Fialho, L., & Novais, M. H. (2024). Floating photovoltaic systems: photovoltaic cable submersion testing and potential impacts. Open Research Europe, 3, 61.
[20] Fan, Y., Meng, J., Ye, H., Wang, P., Wang, Y., & Wang, Y. (2021). Sustainability and ecological efficiency of low-carbon power system: A concentrating solar power plant in China. Journal of Environmental Management, 290, 112659.
[21] Nascimento, E. O., Monteiro, P. R. D., & Borges, T. T. (2023). OPTIMIZATION OF CABLES IN A SOLAR POWER PLANT USING GENETIC ALGORITHMS. International Journal of Advances in Engineering & Technology, 16(6), 608-625.
[22] Min, C. (2018). Computer-Assisted Wiring Optimization Method for Photovoltaic Power Plant Area. American Journal of Modern Energy, 4(3), 17-25.
[23] Akšamović, A., Konjicija, S., Odžak, S., Pašalić, S., & Grebović, S. (2022). DC cabling of large-scale photovoltaic power plants. Applied Sciences, 12(9), 4500.
[24] NAKAGAWA, M., & XIANG, D. (2013). Technology for Large-Scale Photovoltaic Power Generation Systems. Energy Creation Technologies-Power Plants and New Energy, 59(2), 118.
[25] Wang, L., Li, L., Fan, L., Nan, J., Xu, K., Huo, Y., ... & Chen, H. (2022, July). Research on the Insulation Detection Technology of the AC Cable in Distributed Photovoltaic Power Station Considering Photovoltaic Inverter. In 2022 2nd International Conference on Electrical Engineering and Mechatronics Technology (ICEEMT) (pp. 291-295). IEEE.
[26] Ekici, S., & Kopru, M. A. (2017). Investigation of PV system cable losses. International Journal of Renewable Energy Research (IJRER), 7(2), 807-815.
[27] Ebhota, W. S., & Tabakov, P. (2025). Influence of Cabling on Photovoltaic System Performance: Wire Length, Diameter, and Material. Kurdistan Journal of Applied Research, 10(1), 50-65.